BULLETIN OF THE POLISH ACADEMY OF SCIENCES
TECHNICAL SCIENCES, Vol. 65, No. 2, 2017
DOI: 10.1515/bpasts-2017-0021

Microstructure characterization of localized corrosion wear of Cr/Cr_2N+ a-C:H/a-C:H:Cr multilayer coatings on carbon fiber composites

M. JANUSZ[1], L. MAJOR[1]*, J.M. LACKNER[2], B. GRYSAKOWSKI[3], and H. KRAWIEC[3]

[1]Institute of Metallurgy and Materials Science, Polish Academy of Sciences, 25 Reymonta St., 30-059 Kraków, Poland
[2]Institute for Surface Technologies and Photonics, 94 Leobner St., 8712 Niklasdorf, Austria
[3]Faculty of Foundry Engineering, University of Science and Technology, 23 Reymonta St., 30-059 Kraków, Poland

Abstract. The use of carbon fiber composites (CFC) for different applications is widespread. Carbon-based materials show, however, significant oxidative degradation in air. Modern materials are subjected to aggressive, corrosive environment. This type of environment may strongly reduce their mechanical properties. For the protection of CFC, it was necessary to apply coatings to the composite surface. In the presented paper, a chromium/chromium nitride (Cr/Cr2N) multilayer structure has been selected as the inner part. The outer part of the coating was a hydrogenated amorphous carbon (a-C:H), gradually implanted by Cr nanocrystals. The application of transmission electron microscopy (TEM) indicated that the proposed deposition method allowed the formation of a Cr/Cr2N multilayer of Λ = 150 nm, topped with a-C:H+ Cr23C6 composite of a varied carbides density. The micro-hardness of the deposited coatings was up to 14 GPa (at a load of 2 and 5 mN). The microstructure of the deposited coatings was described in detail by means of TEM in the authors' recently published paper [1]. This paper is a continuation thereof, aimed at describing microstructure changes after a localized corrosion process. In order to study localized corrosion in coatings, particularly in metallic (Cr) interlayers, the potential measurements and voltammetry experiments were performed in a Ringer solution. The open-circuit potential reaches stable values after a sufficient time period. The results indicated that the presence of a-C:H+Cr23C6, the outer part of the coating, speeds up the localized corrosion process in Cr interlayers in the inner part of a coating.

Key words: nano-composite multilayer coatings, micro-corrosion, carbon-fiber composites, microstructure characterization, TEM.

1. Introduction

Carbon-based materials show significant oxidative degradation in air, beginning at temperatures in the vicinity of 400°C. The reinforcement of carbon with carbon fibers complicates the anti-oxidative coating problem due to thermal and elastic anisotropy [2].

In many cases, modern materials are also subjected to aggressive, corrosive environment. This type of environment will not affect the CFC substrate composite as it would metallic substrates (corrosion process), however, it can strongly reduce its mechanical properties. Therefore, a coating concept for carbon–carbon composites should consist of an inner part with an ability of stress compensation, which serves as a structural link to the carbon substrate, and an outer part, which acts as an oxide diffusion barrier. Multilayer coatings can lead to benefits in performance over comparable single-layer coatings, and can combine the properties of different materials in one protective coating [3].

In the presented paper, as the inner part, a chromium/chromium nitride (Cr/CrN) multilayer was selected, which recently grabbed strong attention [4–7]. It is characterized by high adhesion and wear and corrosion resistance [5, 6, 8–10].

*e-mail: l.major@imim.pl

The Cr_2N and Cr elementary unit cell of a = 4.14 Å and 2.88 Å respectively, allow a cube-on-cube, local epitaxial growth with a low mismatch (1.6%).

In the presented paper, the outer part of the coating was a-C:H implanted by Cr nanocrystals. It is well-known that hydrogenated amorphous carbon (a-C:H) coatings have low-friction coefficients and low-specific wear rates [11]. Thus, the amorphous carbon coatings are very promising tribo-materials. However, poor adhesion to the substrate, high residual stress, and inherent thermal stability would limit the application of a-C:H coatings [11]. Currently, many metallic elements (Ti, W, Ag, Cr, etc.) have been trialed for modifying the structure of the coatings, and it has been proved that metal doping is an effective method of reducing residual stress and enhancing their adhesion strength [12]. Among those doping metals, Cr, as one part of a carbide, presents an attractive combination of properties (corrosion resistance, wear resistance, etc.) [13, 14].

The discussed materials are designed de novo for elements of surgical tools. Thus, the coatings should be assembled to show resistance to aggressive biological fluids, as well as to be characterized by adequate mechanical properties, namely be wear-resistant. In order to study the localized corrosion behavior of coatings, particularly in metallic interlayers, the open circuit potential (OCP) measurements and linear sweep voltam-

metry experiments were performed in a Ringer solution, which simulated the aggressive biological environment.

The presented paper deals with microstructure changes of the coatings after localized corrosion wear.

2. Experimental procedure

2.1. Deposition procedure. Coatings were prepared using magnetron sputtering technique, with high purity chromium (99.9% at. Cr) and carbon (graphite) targets. The obtained coatings consisted of two parts:

- the inner part, a Cr/Cr_2N multilayer. This part was deposited first on the carbon-fiber-composite substrate material (CFC).
- the outer part, formed from a-C:H matrix gradually implanted by chromium.
- Four different versions of the deposition parameters set of the outer part of the coating were applied. The parameter sets are listed in Table 1.

Table 1
Four different versions of the deposition parameters set, of the outer part of the coating

A variant

Step	Cr [W]	C [W]	C_2H_2 [sccm]	Ar [sccm]	N_2 [sccm]	Time [min]	
1	1400	50	5	45	0	14	1/3
2	1230	410	4,5	45,6	0	14	
3	1060	780	3,8	46,2	0	14	
4	890	1150	3,1	45,2	1,7	14	2/3
5	720	1520	2,5	44,2	3,3	14	
6	550	1890	1,9	43,1	5	14	
7	380	2260	1,3	42	6,7	14	
8	210	2630	0,6	41,1	8,3	14	
9	50	3000	0	40	10	14	

B variant

Step	Cr [W]	C [W]	C_2H_2 [sccm]	Ar [sccm]	N_2 [sccm]	Time [min]	
1	1400	50	5	45	0	14	2/3
2	1230	410	4,5	45,6	0	14	
3	1060	780	3,8	46,2	0	14	
4	890	1150	3,1	45,2	1,7	14	
5	720	1520	2,5	44,2	3,3	14	
6	550	1890	1,9	43,1	5	14	
7	380	2260	1,3	42	6,7	14	1/3
8	210	2630	0,6	41,1	8,3	14	
9	50	3000	0	40	10	14	

C variant

Step	Cr [W]	C [W]	C_2H_2 [sccm]	Ar [sccm]	N_2 [sccm]	Time [min]	
1	1400	50	20	30		14	2/3
2	1230	410	22,5	27,5		14	
3	1060	780	25	25		14	
4	890	1150	27,5	22,5		14	
5	720	1520	30	20		14	
6	550	1890	32,5	17,5		14	
7	380	2260	35	15		14	1/3
8	210	2630	37,5	12,5		14	
9	50	3000	40	10		14	

D variant

Step	Cr [W]	C [W]	C_2H_2 [sccm]	Ar [sccm]	N_2 [sccm]	Time [min]	
1	1400		20	30		14	2/3
2	1230		21,9	28,1		14	
3	1060		23,8	26,2		14	
4	890		25,6	24,4		14	
5	720		27,5	22,5		14	
6	550		29,4	20,6		14	
7	380		31,2	18,8		14	1/3
8	210		33,1	16,9		14	
9	50		35	15		14	

Numbers 1 to 9 correspond to nine a-C:H layers implanted by Cr, from bottom to top. Details of the deposition process are given in [15, 16].

2.2. Microstructure characterization. The microstructure of the coatings was carried out by a Tecnai G^2 F20 FEG (200 kV) transmission electron microscope (TEM) in a bright field technique (BF), as well as using scanning mode (STEM images) by the application of high-angle annular dark-field STEM detector (HAADF). Phase analysis was performed through electron diffraction pattern. Energy-dispersive spectroscopy (EDS) was used for chemical analysis. Thin foils were prepared using focused ion beam (FIB) (Quanta 200 3D) equipped with an OmniProbe in-situ lift-out system. All thin foils were cut as cross-sections of the investigated coatings.

2.3. Micromechanical analysis. Micromechanical tests were connected with micro-hardness, as well as with the elastic modulus measurements using a Berkovich indenter loaded with 2 and 5 mN.

2.4. Localized corrosion experiments. In the presented paper, the corrosion process was studied only in the coating zone, in particular in the metallic interlayers. It allowed to analyze the coating's ability to protect the substrate against aggressive fluids. The process was called localized micro-corrosion because it was analyzed in a micro-scale. The localized micro-corrosion (electrochemical) behavior of samples was tested in isotonic to human tissue Ringer's solution, at a temperature same as human core temperature (37°C), and pH = 7.2, the pH of human body fluids. Open circuit potential (OCP) curves and polarization curves (linear sweep voltammetry, LSV) were recorded versus an Ag/AgCl (KCl sat.) reference electrode with the use of an Autolab PGStat 302N potentiostat/galvanostat. A platinum electrode was used as the counter electrode in LSV experiments, and the potential was scanned in a range from –1000 to 1500 mV versus Ag/AgCl (KCl sat.), at a rate of 1 mV/s.

3. Results and discussion

3.1. Microstructure characterization of the deposited Cr/Cr_2N + a-C:H + Cr nano multilayer coating on a carbon fiber composite material. The microstructure of the coating was shown in the bright field TEM image (Fig. 1).

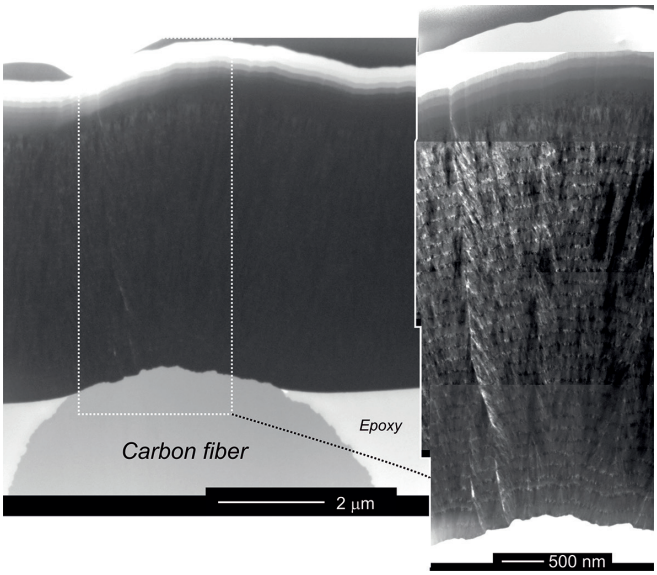

Fig 1. Microstructure analysis of nano-composite multilayer coating on the cross- section by TEM bright field technique [1]

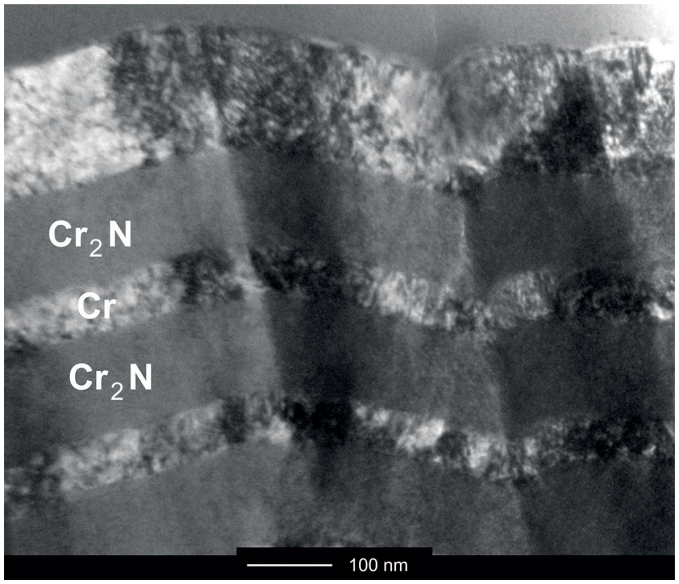

Fig. 2. Microstructure characterization of the Cr/Cr_2N part of the coating (the inner part) presenting details of local inheritance of orientations (TEM bright field analysis) [1]

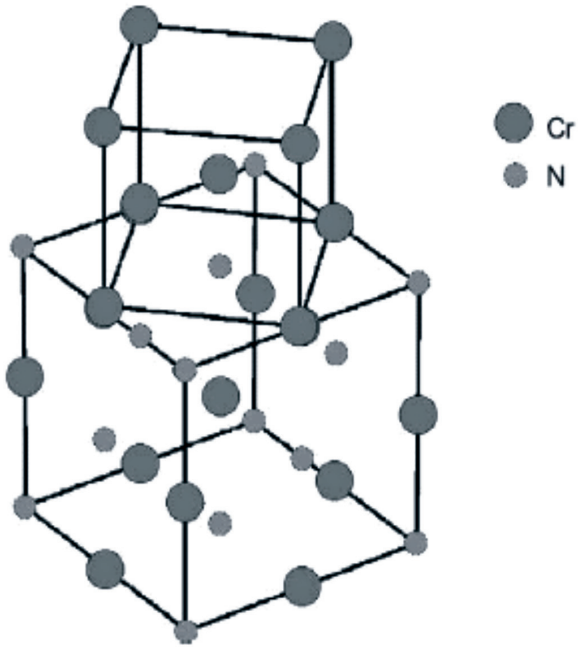

Fig. 3. Scheme of Cr and Cr_2N unit cell relation [7]

The microstructure of the deposited coating (before the localized corrosion process) was described in detail in the author's recently published paper [1].

In the inner part of the coating, a Cr/Cr_2N multilayer formed, which showed a pseudo-columnar structure, indicating that locally, the crystallographic relation is retained (the same diffraction contrast went through several interfaces at a time) (Fig. 2) [1].

There is a possibility of cube-on-cube grain growth in the [1 0 0] direction perpendicular to the interfaces, where Cr and Cr_2N cells fit properly with relatively low lattice parameter mismatch (~1.6%), as presented in Fig. 3 [7].

3.2. Micromechanical properties of analyzed coatings. The microstructure characterization and phase identification by SAED revealed that $Cr_{23}C_6$ carbides were present in the coating. The $Cr_{23}C_6$ are characterized by high hardness (Vicker's micro-hardness of 976 MPa), while pure a-C:H had a much lower hardness (750 MPa) [17–21]. In majority, it is characterized by sp^2 bonds [22]. During the wear process, because of the presence of a relatively soft phase at the surface of the coating, the mechanical contact would be much better.

Implantation of amorphous carbon by chromium carbides might nearly double the micro-hardness and treble the elasticity modulus (Fig. 4).

The coating D was not mechanically tested, due to the fact that the a-C:H part thereof delaminated just after the deposition process because of the high residual stress formed at the interface with the inner part of the coating.

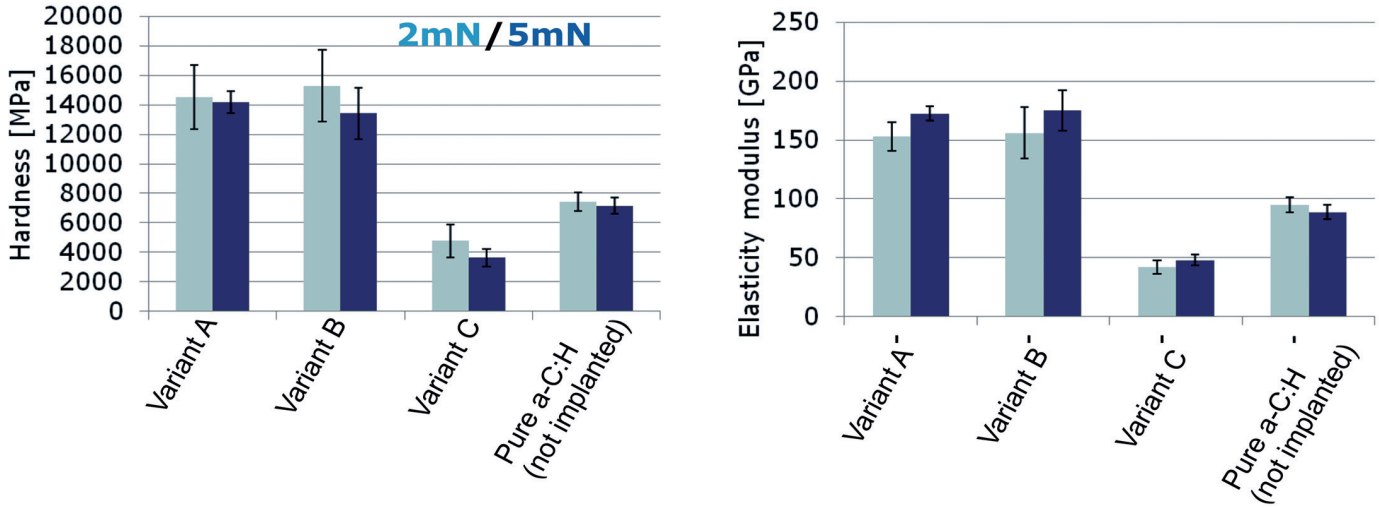

Fig. 4. Effect of deposition conditions on micro-hardness and elasticity modulus of coatings

3.3. Localized corrosion analysis and microstructure change characterization of coatings after the corrosion test. In order to study the localized micro-corrosion behavior of coatings, in particular of the metallic interlayers, open circuit potential (OCP) measurements and linear sweep voltammetry experiments were performed in Ringer solution. It is worth mentioning that OCP values suggest a more noble behavior of the investigated coatings compared to values of corrosion potential registered in LSV experiments.

The shapes of anodic branches of the registered polarization curves (Figs. 5, 6) suggest that coating D corrodes actively, with lower, comparing to coatings A and B, current density values at potentials in range from corrosion potential to 200 mV or 300 mV (versus Ag/AgCl KCl sat.), whereas for coatings A and B, large anodic peaks were observed.

Those peaks were related to the rapid corrosion (dissolution) of layers, manifested by an increase in current density values, followed by a decrease in the observed current density due to formation of a continuous layer of corrosion products covering the active sites in Cr/Cr_2N layers. At higher potentials, all coatings underwent active dissolution, and lower current density values registered for samples A, B, and C indicated higher susceptibility to corrosion.

The SEM image of the surface of sample A, taken after linear sweep voltammetry (LSV) experiments, suggests that coating corrosion started in the cracks in the coating, what was indicated by the presence of dark areas in the vicinity of those cracks (Fig. 7).

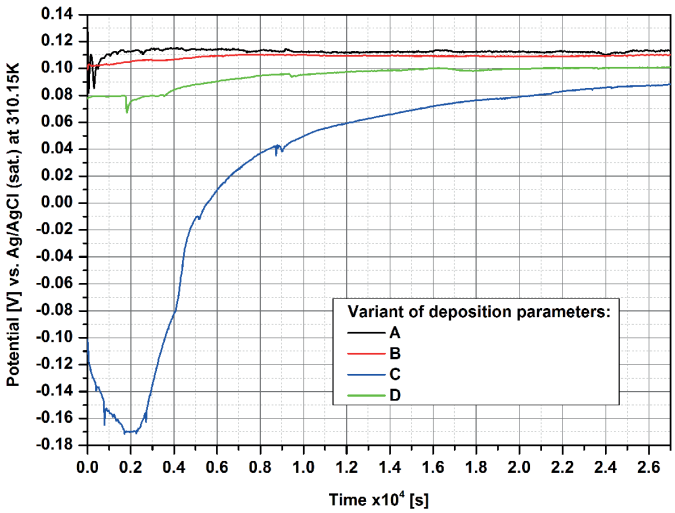

Fig. 5. Open circuit potentials measured for specimens as a function of immersion time in Ringer solution at 37°C

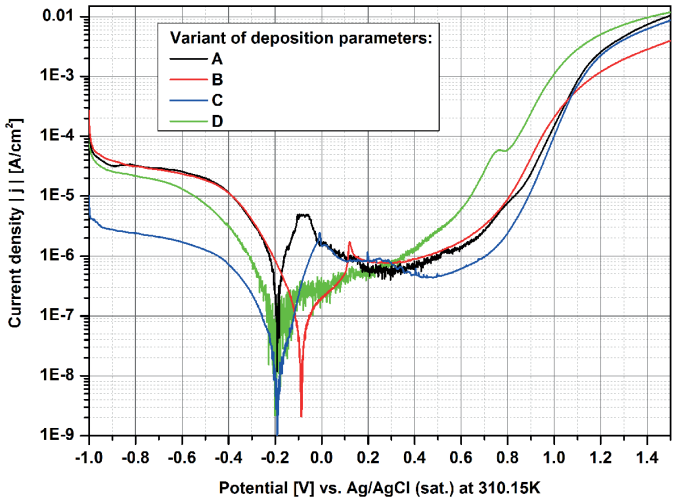

Fig. 6. Polarization curves recorded for all samples with a potential scan rate of 1 mV/s in Ringer solution at 37°C

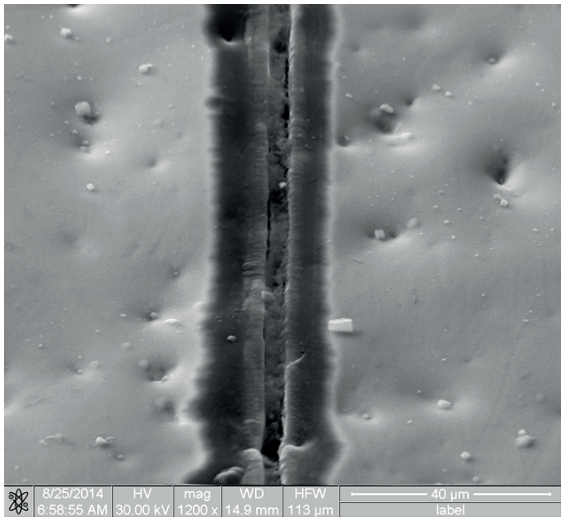

Fig. 7. SEM image of the crack on the surface of sample A

Analysis of cross-sections in TEM bright field mode, revealed that the outer a-C:H part of the coating remained intact, and due to the penetration of Ringer's solution through the cracks, the inner Cr/Cr_2N layers underwent degradation processes and large voids covered with corrosion products were formed (Fig. 8).

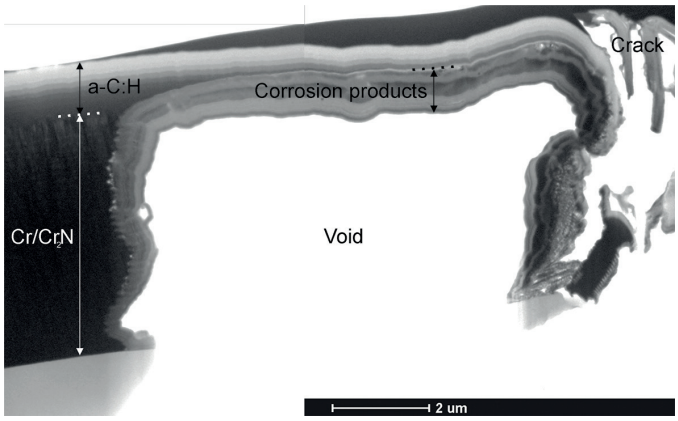

Fig. 8. A void formed under the most outer chromium implemented a-C:H layer due to penetration of Ringer's solution through crack. TEM bright field image done after LSV experiment

It was also clearly visible that the layers most susceptible to corrosion were the Cr ones (Fig. 9) – small and slightly elongated cavities were observed at the boundaries between the Cr layers and the corrosion product. This system resembles a pitting corrosion system.

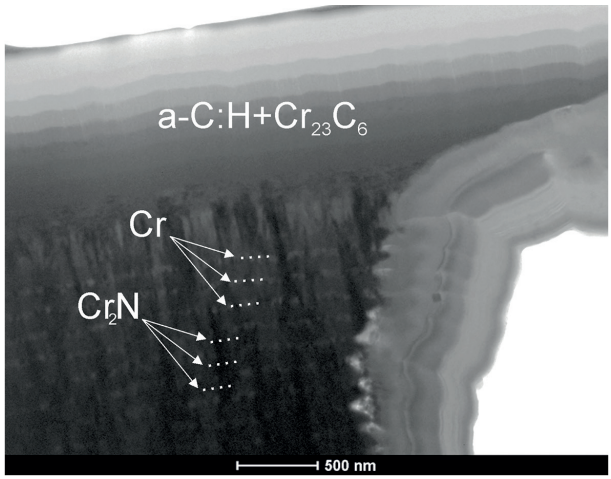

Fig. 9. Detailed microstructure characterization of corrosion product layers formed on the surface of the void, done at the cross-section by TEM bright field technique

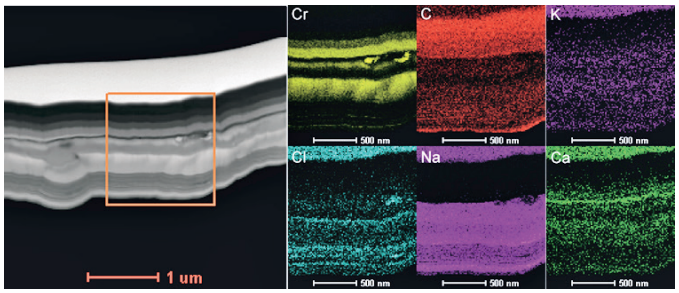

Fig. 10. EDS qualitative chemical analysis of element distribution in coating layers and corrosion products layers

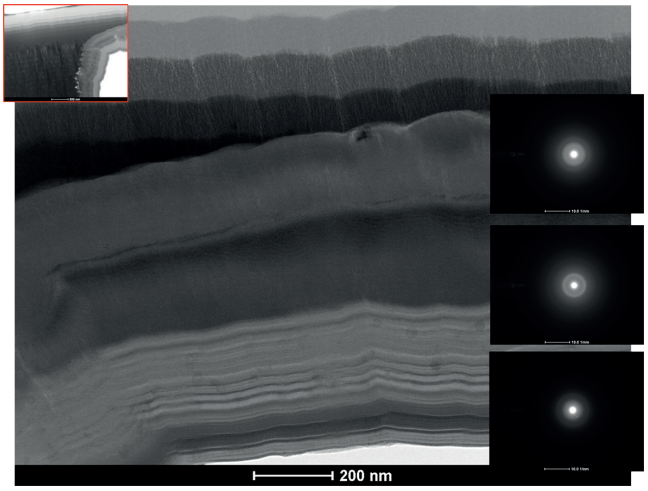

Fig. 11. Analysis of corrosion products deposited on the surface of the void made with TEM bright field as well as selected area electron diffraction techniques

Corrosion products formed a system of layers which differed in chemical composition as well as in distribution of elements (Fig. 10), and exhibit amorphous structure (Fig. 11), what was confirmed by the electron diffraction pattern.

EDS qualitative chemical analysis revealed that the concentration of chromium was the highest in the middle layer of corrosion products with almost linear concentration profile (Fig. 12), and in small voids on the boundary between the outer layer of corrosion products and the a-C:H coating.

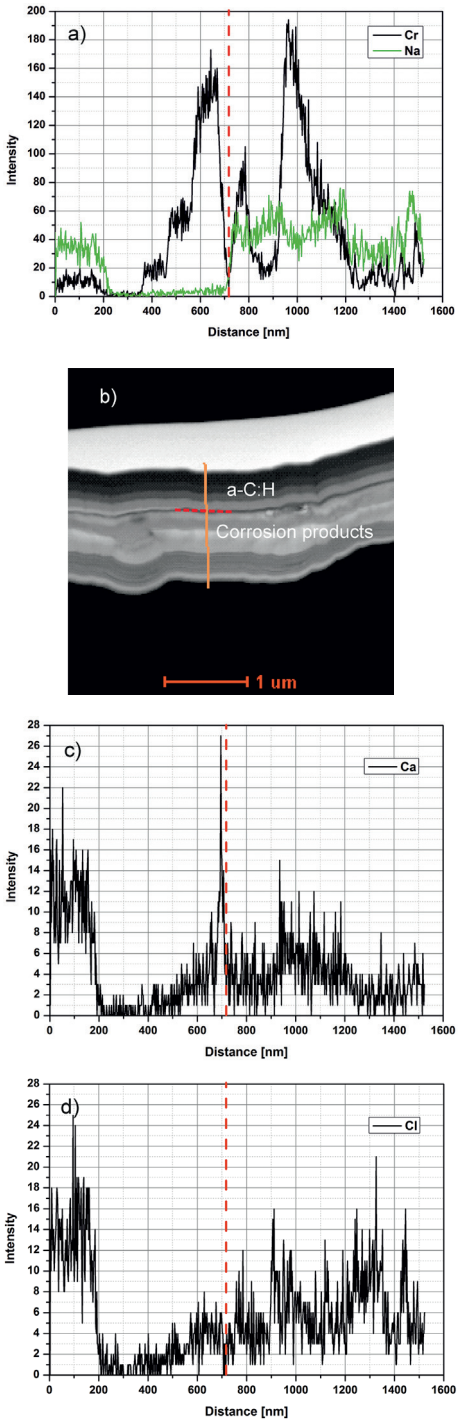

Fig. 12. STEM-EDS qualitative chemical analysis of chromium, sodium, calcium and chlorine concentration measured along a line

The highest chlorine and calcium concentrations were observed on the boundaries between corrosion products layers and between the outermost corrosion products layer and the a-C:H coating respectively (Fig. 12d). It is postulated that uneven distribution of elements in corrosion product layers was a result of pH changes in the solution filling the cavities (pits) during the corrosion processes. In aerated solution of pH ≈ 7.20, chromium undergoes oxidation to Cr_2O_3 and partially to $Cr(OH)_3$. When the pH of the solution in the cavity (pit) gradually decreases, due to reaction , amphoteric chromium (III) hydroxide reacts according to reaction , forming soluble Cr^{3+} ions [23].

$$2CrC_x + 3H_2O \rightleftharpoons Cr_2O_3 + 2xC + 6H^+ + 6e^- \quad (1)$$

$$Cr(OH)_3 + 3H^+ \rightleftharpoons Cr^{3+} + 3H_2O \quad (2)$$

This process presumably explains the uneven chromium distribution in the middle layer of corrosion products (Fig. 12).

Sodium atoms were distributed unevenly across the corrosion products – its concentration changes linearly across a single corrosion products layer (Fig. 12a). Comparison of sodium and chromium concentration profiles (Fig. 12a) indicated that sodium concentration reached highest values in the areas of lower chromium concentration. High concentration of calcium was found on the boundary between the a:C-H layer and the corrosion products layer. The highest concentration of chloride ions was found on the boundary between the corrosion products layers, mostly between the outermost and middle layers of corrosion products.

Different electrochemical behavior was observed in the case of sample D covered with the poorly adhering a-C:H layer (which was removed due to the presence of residual stresses, Fig. 13).

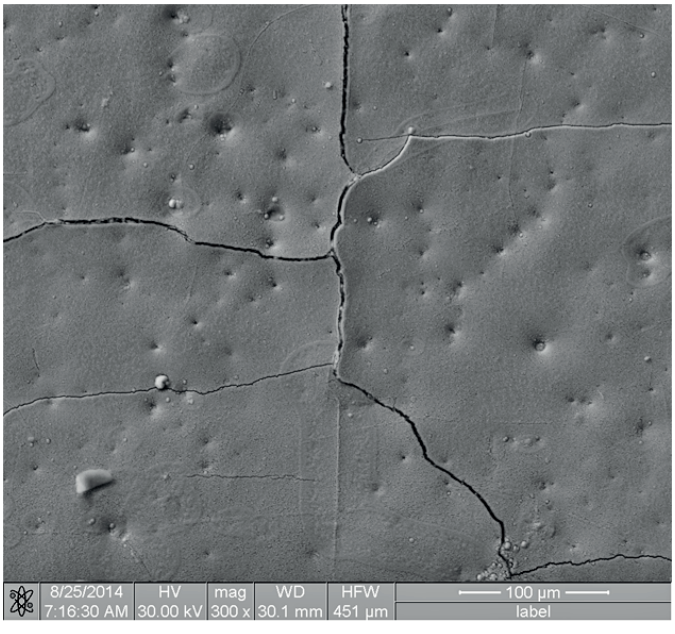

Fig. 13. SEM image of cracks formed in the multilayer deposited on the surface of sample D

As for sample A, corrosion starts in the cracks in the Cr/Cr_2N multilayer, but in contrast to the previous mechanism, the cavities were not observed and a V-shaped crevice was formed. The walls of the crevice were covered with corrosion products under which bent Cr_2N layers (rib-like structures) were found (Fig. 14).

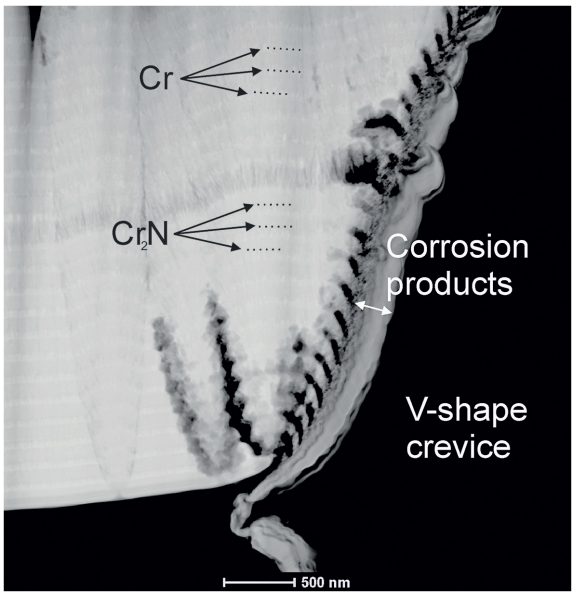

Fig. 14. STEM image of the rib-like structure covered with corrosion products formed in the V-shape crevice in the multilayer of sample D

The layers most susceptible to corrosion are the Cr layers.

4. Conclusions

The application of transmission electron microscopy allowed to show that:

- magnetron sputtering technique allowed for the formation of dedicated nano-structured (the inner Cr/Cr_2N and the outer a-C:H+ $Cr_{23}C_6$) multilayers
- the gradient implantation of a-C:H by chromium caused the formation of a layered nano-composite structure in the outer part of the coating
- co-deposition of chromium and a-C:H resulted in the formation of ($Cr_{23}C_6$) nano-particles
- introduction of carbide nano-particles into the a-C:H part of the coating and connecting it with the Cr/Cr_2N multilayer allowed to double the a-C:H hardness and treble its elastic modulus
- for coatings deposited with the use of A and D variants of deposition parameters, open circuit potential reaches stable values after a sufficient period of time, whereas for samples B and C, open circuit potential values increase gradually in time.

Acknowledgements. The research project was financed by the National Science Centre (Polish – Narodowe Centrum Nauki, abbr. NCN)No: 2012/06/M/ST8/00408

References

[1] L. Major, M. Janusz, J.M. Lackner, M. Kot, and B. Major, "Microstructure characterization of advanced protective Cr/CrN+a--C:H/a-C:H:Cr multilayer coatings on carbon fibre composite (CFC)", *Journal of Microscopy* 262, 191–202 (2016).

[2] E. Fischer, "A simple model of the a-axis conductivity in graphite intercalation compounds", *Carbon* 16, 161–163 (1977).

[3] L. Major, J.M. Lackner, and B. Major, "Bio-tribological TiN/Ti/a--C:H multilayer coatings development with a built-in mechanism of controlled wear", *RSC Adv*. 4, 21108–21114 (2014).

[4] L. Major, W. Tirry, and G. Van Tendeloo, "Microstructure and defect characterization at interfaces in TiN/CrN multilayer coatings", *Surf. Coat. Technol*. 202, 6075–6080 (2008).

[5] M. Berger, U. Wiklund, M. Eriksson, H. Enqvist, and S. Jacobson, "The multilayer effect in abrasion: Optimising the combination of hard and tough phases", *Surf. Coat. Technol*. 116–119, 1138–1144 (1999).

[6] H.A. Jehn, "Improvement of the corrosion resistance of PVD hard coating – substrate systems", *Surf. Coat. Technol*. 125, 212–217 (2000).

[7] S. Han, J.H. Lin, X.J. Guo, S.H. Tsai, Y.O. Su, J.H. Huang, F.H. Lu, and H.C. Shih, "Effect of Cr interlayer on the microstructure of CrN coatings on steel", *Thin Solid Films* 377–388, 578–584 (2000).

[8] L. Major, J. Morgiel, B. Major, J.M. Lackner, W. Waldhauser, R. Ebner, L. Nistor, and G. Van Tendeloo, "Crystallographic aspects related to advanced tribological multilayers of Cr/CrN and Ti/TiN types produced by pulsed laser deposition (PLD)", *Surf. Coat. Technol*. 200, 6190–6195 (2006).

[9] S. Han, J.H. Lin, D.Y. Wang, F.-H.Lu, and H.C. Shih, "Corrosion resistance of chromium nitride on low alloy steels by cathodic arc deposition", *J. Vac. Sci. Technol*. A 19 (4), 1442–1446 (2001).

[10] D.K. Merl, P. Panjan, M. Cekada, and M. Macek, "The corrosion behavior of Cr-(C,N) PVD hard coatings deposited on various substrates", *Electrochim. Acta* 49, 1527–1533 (2004).

[11] H. Ronkainen, S. Varjus, and K. Holmberg, "Friction and wear in dry, water- and oil-lubricated DLC against alumina and DLC against steel contact", *Wear* 222, 120–128 (1998).

[12] Q. Wang, F. Zhou, X. Ding, Z. Zhou, C. Wang, W. Zhang, L. Kwok-Yan Li, and S. Tong Li, "Structure and water-lubricated tribological properties of Cr/a-C coatings with different Cr content", *Tribol. Int*. 67, 104–115 (2013).

[13] MS. Zimowski, T. Moskalewicz, M. Kot, B. Wendler, and A. Czyrska-Filemonowicz, "Microstructure, mechanical and tribological properties of the nc-Cr_xC_y/a-C and nc-Cr_xC_y/a-C:H nanocomposite coatings on oxygen-hardened Ti-6Al-4V alloy", *Surf. Inter. Anal*. 44, 1225–1228 (2012).

[14] T. Moskalewicz, B. Wendler, and A. Czyrska-Filemonowicz, "Microstructural characterisation of nanocomposite nc-MeC/a-C coatings on oxygen hardened Ti-6Al-4V alloy", *Mater. Character*. 61, 959–968 (2010).

[15] J.M. Lackner, "Industrially-scaled large-area and high-rate tribological coating by pulsed laser deposition", *Surf. Coat. Technol*. 200, 1439–1444 (2005).

[16] J.M. Lackner, W. Waldhauser, R. Berghauser, R. Ebner, and G. Kothleitner, "Growth phenomena in room temperature pulsed laser deposited chromium and chromium nitride coatings", *Surf. Coat. Technol*. 200, 387–390 (2005).

[17] H.O. Pierson, *Handbook of Refractory Carbides and Nitrides*, Noyes Publications, 1996.

[18] M. Kot, L. Major, and J.M. Lackner, "The tribological phenomena of a new type of TiN/a-C:H multilayer coatings", *Mater. and Design* 51, 280–286 (2013).

[19] M. Kot, L. Major, K. Chronowska-Przywara, J.M. Lackner, W. Waldhauser, and W. Rakowski, "The advantages of incorporating CrxC nanograins into an a-C:H matrix in tribological coatings", *Mater. and Design* 56, 981–989 (2014).

[20] A. Czyżniewski, "Preparation and characterisation of a-C and a-C:H coatings deposited by pulsed magnetron sputtering", *Surf. Coat. Technol*. 203, 1027–1033 (2009).

[21] G. Gassner, P.H. Mayrhofer, C. Mitterer, and J. Kiefer, "Structure–property relations in Cr–C/aC:H coatings deposited by reactive magnetron sputtering", *Surf. Coat. Technol*. 200, 1147–1150 (2005).

[22] J.M. Lackner, C. Stotter, W. Waldhauser, R. Ebner, W. Lenz, and M. Beutl, "Pulsed laser deposition of diamond-like carbon coatings for industrial tribological applications", *Surf. Coat. Technol*. 174–175, 402–407 (2003).

[23] J. Högström, M. Andersson, U. Jansson, F. Björefors, and L. Nyholm, "On the evaluation of corrosion resistances of amorphous chromium–carbon thin-films", *Electrochim. Acta Mater*. 122, 224–233 (2014).